Chemical Engineering Journal 157 (2010) 146–160

Contents lists available at ScienceDirect

Chemical Engineering Journal

journal homepage: www.elsevier.com/locate/cej

Hydrodynamics and mass transfer characteristics in an inverse internal loop airlift-driven fibrous-bed bioreactor

Peter M. Kilonzo, Argyrios Margaritis*, M.A. Bergougnou

Department of Chemical and Biochemical Engineering, University of Western Ontario, London, Ontario N6A 5B9, Canada

ARTICLE INFO

Article history:
Received 10 August 2009
Received in revised form
12 November 2009
Accepted 17 November 2009

Keywords:
Fibrous-bed
Airlift bioreactor
Gas holdup
Liquid circulation velocity
Oxygen mass transfer

ABSTRACT

In this work, the hydrodynamic and mass transfer characteristics were studied in an internal loop airlift-driven bioreactor (ILALB) with and without fibrous-bed packing. Woven cotton and/or polyurethane foam were inserted in the downcomer section of the ILALB to represent the fibrous-bed. Gas holdup and K_La values continuously increased with decrease in gap width, but with increases in both packing height and bed's top clearance. This was associated with the increase in the interfacial area due to the shearing action of the fibrous-bed. Increased amounts of packing in the ILALB, whether cotton or polyurethane foam in the form of height with large top clearance and narrow gap width, decreased the liquid circulation velocity in the ILALB because of increased frictional resistance, tortuosity, and baffling action of the bed. Empirical correlations are presented which accurately predict gas holdup, liquid circulation velocities, and volumetric mass transfer coefficient as a function of all five independent variables (packing nature, packing height, bed's top and bottom clearances, gap width, and gas velocity). The optimum hydrodynamic conditions to improve mass transfer were observed at full packing with large bed top clearance and 0.004 m gap width between fiber surfaces.

1. Introduction

Three-phase internal loop airlift (TPILAL) bioreactors involving particles have been increasingly gaining popularity in biotechnology industry at both production and research scale because of their simple mechanical design and effective gas–liquid and liquid–solid phase contact [1–7]. In recent years, because of innovation and advancement in molecular biology, airlift reactors with packed bed have also attracted much attention because of their low cost, potential for high cell density and preferential retention of cell type leading to bioreactor stability [8,9]. These devices are constantly being applied in aerobic fermentation systems due to their low contamination level and the liquid circulation velocity induced by the difference of hydrostatic pressure leading to a uniform and sufficient mixing for microbial reactions at low power input [10,11]. Indeed, conventional packed bed systems often suffer from poor long-term stability due to reactor bed clogging, flow channeling, cell degeneration, high pressure drop, and poor mass transfer.

Recently, fibrous materials (cotton, polyester, glass, nylon, ryon, polymer foam and sponge) have proven to be suitable for aerobic packed bed bioreactor [12,13] packing, since they provide high specific surface area for cell attachment, high and constant surface-to-volume ratio, leading to both smaller pressure drops and lower mass transfer resistance as compared to micro-carrier particles, high void volume, low cost, high mechanical strength, and high permeability [14–16]. Also, their availability, maximum loading, low diffusion problems, nontoxicity, biodegradability, and durability make fibrous matrices more attractive for cell support [14,15,17–19]. The spiral wound bed configuration with gaps between two adjacent layers of the fibrous sheet matrix allows improved multiphase flow, minimal diffusion limitations, and renewable surface for cell immobilization. However, the success of such bioreactor design depends on the ability of the airlift to drive the liquid through the packing at the required rate, which depends on the need to attain particular levels of solid–liquid mass transfer in the packing. On the other hand, the liquid circulation velocity through the fibrous-bed structure may be employed to control cell detachment and biofilm development. Such an approach would be beneficial to clogging problems.

Hydrodynamic and mass transfer characteristics in airlift bioreactors with packed beds are a complex function of the physical properties of the system, the operating conditions, and the bioreactor geometry. Therefore, experimental data are required in order to enhance the packing efficiency. Chisti and Moo-Young [21] studied the improvement of gas–liquid mass transfer in an ELALB ($V_L \cong 15$ L, $h_L = 1.8$ m, $A_r/A_d = 0.444$, $U_{gr} = 0$–0.12 m s^{-1}) using Sulzer SMV-12 motionless mixer elements in the riser section. Chisti and Moo-Young (1993) have also studied liquid circulation velocity in an external loop airlift bioreactor (ELALB)

* Corresponding author. Tel.: +1 519 661 2146; fax: +1 519 661 3498.
E-mail address: amarg@uwo.ca (A. Margaritis).

1385-8947/$ – see front matter © 2009 Elsevier B.V. All rights reserved.
doi:10.1016/j.cej.2009.11.023

Nomenclature

a	interfacial area (m^2/m^3)
A	cross-sectional area (m^2)
m_P	gap width between adjacent fiber surfaces (m)
C_L	concentration, in liquid phase (mg/L)
C_L^*	dissolved oxygen concentration in equilibrium with oxygen in the gaseous phase (mg/L)
d	diameter (m)
f	frictional loss coefficient
E	energy loss in the reactor (W)
D_L	axial dispersion coefficient (m^2/s)
g	gravitational acceleration (m^2/s)
h	height (m)
H	Henry's constant (atm L)/(mg K)
K_H	permeability (m^2)
K_L	liquid-side mass transfer coefficient ($m\,s^{-1}$)
K_La	volumetric mass transfer coefficient (s^{-1})
L	height (m)
M	molecular weight (g/mol)
P	pressure/port
Q	flow rate ($m^3\,s^{-1}$)
r	radius (m)
R	regression coeffient
Re	Reynolds number
s	gas–liquid separator of bioreactor as shown in Fig. 3
S_U	specific surface area of the support element ($m^2\,m^{-3}$)
t	instantaneous time (s)
T	temperature
U	superficial velocity ($m\,s^{-1}$)
u	linear velocity ($m\,s^{-1}$)
V	volume (m^3)
x	x-coordinate (m)
y	y-coordinate (m)
z	axial distance (m)
Z	dimensionless concentration

Greek letters

ΔP	pressure drop (Pa)
Δt	time difference (s)
Φ	empirical constant as given in Eq. (31)
Ψ_o	pore distribution (pores/m^2)
α	empirical coefficient as given in Eq. (12a)
β	empirical coefficient as given in Eq. (12a)
ε	gas holdup
ϕ	porosity
μ	viscosity (Pa s)
ρ	density (kg/m^3)
ξ	empirical constant as given in Eq. (31)
ω_{O_2}	mole fraction of oxygen

Subscripts

av	average
avm	average modified
b	bottom
B	bubble
C	column
c	circulation
d	downcomer
D	dispersion
f	friction
g	gas
h	hydraulic
H_2O	water
I	interstitial
L	liquid
M	manometer
m	modified
m_p	gap width
N	sparger
o	pore/orifice
O_2	oxygen
p	packing
r	riser
s	sauter
S	separator
t	top
T	total

(h_L = 8 m, A_r/A_d = 1.0, $0 \le L_p \le 4$ m, $0 \le U_{gr} \le 0.12\,m\,s^{-1}$) using spherical beads ($0.002 \le d_p \le 0.01$ m) and Raschig rings ($0.006 \le d_p$ (nominal) ≤ 0.01 m) in the riser section. Using a 1 m deep of 0.002 m diameter spherical beads at $U_{gr} = 0.01\,m\,s^{-1}$, the liquid velocity dropped to a low value of $0.008\,m\,s^{-1}$. Okada et al. [22] have studied mass transfer in an ELALB column (d_r/d_d = 0.14 m, L_r = 2.67 m, $0.05 \le L_p \le 0.4$ m) using steel pall ring (d_p = 0.015 m) in the riser section. They observed increased K_La value in the presence of static mixers for the liquids used. Nikakhtari and Hill [23] have studied oxygen mass transfer in an ELALB (V_L = 12 L, L_p = 1.2 m, ϕ_p = 0.99, h_L = 1.45 m, d_r = 0.089 m, d_d = 0.047 m, L_d = 1.81 m, A_r/A_d = 3.575, constant $U_{gr} = 0.00147\,m\,s^{-1}$) using woven nylon mesh packing in the riser section. They found that using a constant superficial gas velocity of $0.00147\,m\,s^{-1}$, the K_La value had increased from $0.0011\,s^{-1}$ (unpacked) to $0.0042\,s^{-1}$ in the packed ELALB. In a similar related study, Nikakhtari and Hill [24] have also studied hydrodynamic and mass transfer characteristics in the same ELALB (V_L = 12 L, L_p = 1.2 m, ϕ_p = 0.99, h_L = 1.42 m, d_r = 0.089 m, d_d = 0.047 m, L_d = 1.81 m, A_r/A_d = 3.57, constant $0 \le U_{gr} \le 0.021\,m\,s^{-1}$) using stainless steel mesh (ϕ_p = 0.99). They observed increased gas holdup, decreased bubble size, and decreased liquid circulation velocity in the presence of the packing. However, they noticed that the K_La had increased, approaching a value of $0.021\,s^{-1}$ at high gas velocity. Recently, Martinov et al. [25] studied gas-liquid mass transfer in a laboratory-scale fixed bed reactor column (V_L = 6 L, L_p = 0.26 m, ϕ_p = 0.99, h_L = 0.75 m, d_c = 0.1 m, $0 \le U_{gr} \le 0.021\,m\,s^{-1}$, $0 \le U_L \le 0.0126\,m\,s^{-1}$) with co-current liquid recycling, using PEVA fibrous packing. They observed an increase in K_La value from $0.01\,s^{-1}$ (unpacked) to $0.026\,s^{-1}$ in the packed column. However, very little or no information exists on hydrodynamic and mass transfer characteristics when an internal loop airlift bioreactor (ILALB) is combined with a packed bed, especially in the same column [26,27].

In the present study, the hydrodynamic and mass transfer characteristics of an inverse (annulus sparged) internal loop airlift bioreactor (ILALB) with fibrous-bed, using cotton and/or polyurethane foam packing are analyzed. Correlations were obtained to allow estimation of the gas holdup, liquid circulation velocity, and volumetric gas–liquid mass transfer coefficient with good accuracy of predicting the experimental results.

2. Experimental apparatus and methods

Experiments were carried out using an internal loop airlift-driven fibrous-bed bioreactor shown in Fig. 1. The bioreactor (1) consisted of Plexiglas (poly-methyl methacrylate) column of 0.102 m internal diameter with a water jacket for the temperature

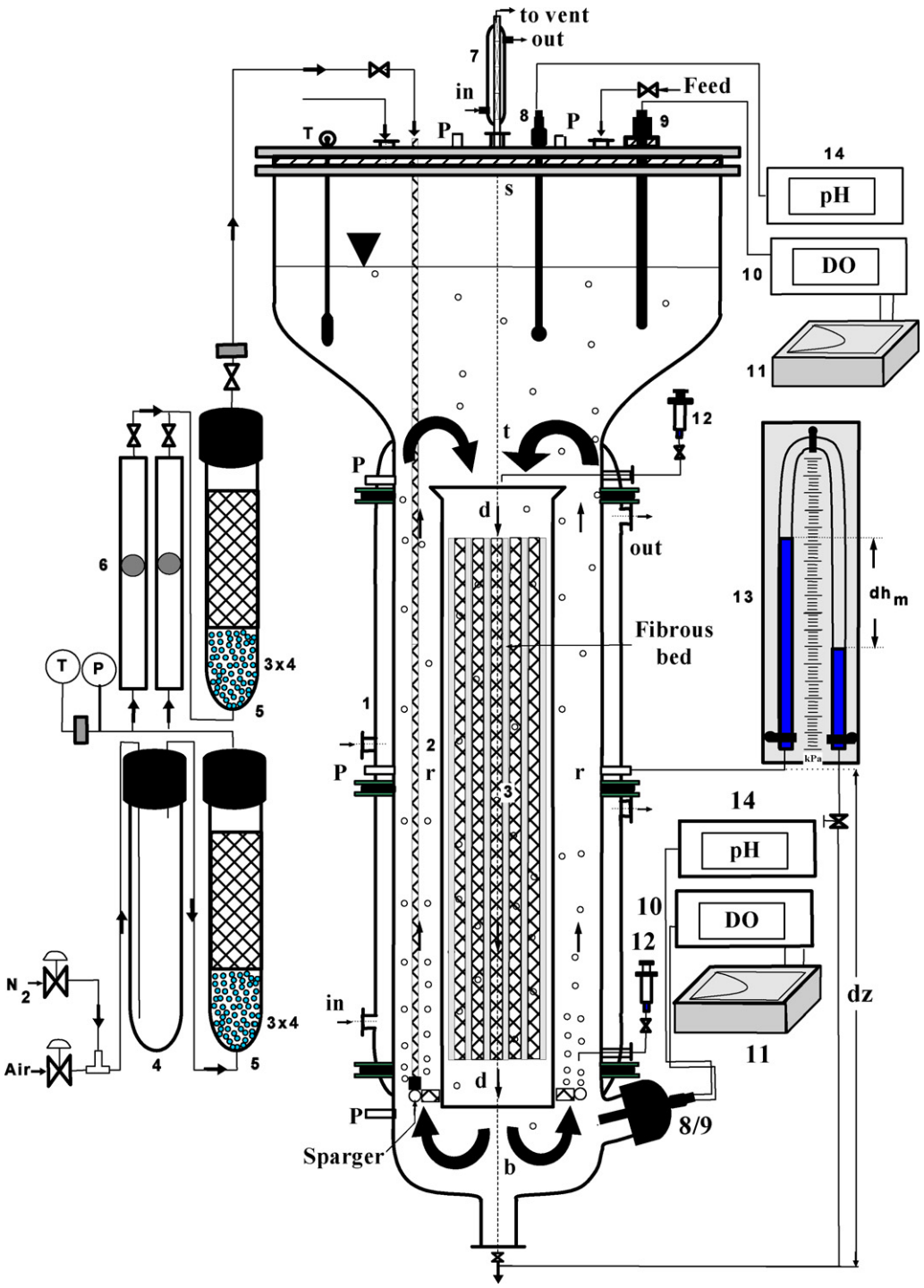

Fig. 1. Schematic diagram of internal loop airlift bioreactor (ILALB) with the fibrous bed packing. 1-Column, 2-draught tube, 3-fibrous-bed, 4-stabilizer, 5-filter, 6-rotameter, 7-condenser, 8-pH electrode, 9-DO electrode, 10-pH meter, 11-recorder, 12-sampling point, 13-manometer, 14-DO meter, b-bottom, d-downcomer, r-riser, t-top, S-separator.

control and an expanded gas-liquid separator (s) (0.257 m I.D. and 0.30 m high) at the top (t) region for efficient gas bubble disengagement. The column also contained an internal concentric draft tube (2) or downcomer section (d) of 0.06 m I.D. and 1.02 m long.

Heavy bleached woven cotton sheets of dimensions 0.69 m × 0.94 m × ~0.0008 m (porosity of 96%, density 800 kg/m^3) and polyurethane foam (PUF) sheets of 0.69 m × 0.94 m × 0.004 m (porosity of 96%, density 30 kg/m^3) were used as the fibrous materials. A stainless steel wire cloth topped with the fibrous cotton or polyurethane sheets was wound into a spiral configuration along the vertical axis. The spiral wound configuration had m_p = 0.002–0.004 m gaps between two adjacent layers of the fibrous sheet matrix to allow fluid flow through the bioreactor unhindered. The fibrous sheet material and the stainless steel mesh also created high specific surface area and porosity (~0.935). These properties produce the lowest flow resistance and allow larger amounts of biomass to attach on the fibrous-bed [28]. Furthermore, high porosity minimizes problems due to plugging during cell cultures.

The spirally wound fibrous matrix was loosely packed in the draft tube section of the airlift reactor. The draft tube incorporating the fibrous matrix packing (3) was positioned within the reactor

column using short stainless steel baffles and held vertically from the upper end using stainless steel rods. The bottom clearance h_b between the draft tube bottom and the base plate was kept constant at 0.059 m. The column also had a bottom section (b) in which the sparger was housed within the riser region (R). The height of the section between the sparger and the liquid level was varied between 1.121 m and 1.158 m. Thus; the active volume was varied between 12 L and 15 L, respectively. The riser-downcomer combination gave a bioreactor column volume of about 6 L and an area ratio A_r/A_d of 1.84. The aspect ratio ($L_{r/d}/d_c$) of the bioreactor was 10. This ratio value was based on the riser or downcomer height (neglecting the liquid level in the separator) and the column diameter (d_c) [9,11,29]. Several holes along the column height and on the top served as pressure taps or sampling and/or tracer injection ports (P).

Pressurized air supplied through a system of pressure buffer and stabilizer (4) was used as the dispersed phase. The air was first filtered using glass wool packed in eight-glass columns (5) and arranged in series, before it was humidified (6) and metered through rotameters (7). Both pressure (P) and temperature (T) of the gas stream were monitored just downstream the rotameters. The air was introduced at the base of the riser from the top through an O-ring distributor made of 0.076 m-diameter stainless steel ring tubing and having 24, $d_o = 8.0 \times 10^{-4}$ m holes equidistantly spaced 0.011 m along the circumference, giving a free area of 0.23% of the total cross-section area of the riser. These holes were facing upward. The distributor was kept 0.019 m just above the bottom end of the draft tube (downcomer region) and held vertically $h_N = 0.083$ m above the bioreactor base plate. The bioreactor was designed with two mounting ports for the DO_2 and/or pH electrodes. One electrode was housed 0.073 m from the base plate (8/9), almost in the same level with the lower end of the draft tube. The second was inserted into the gas–liquid separator (s) from the bioreactor top with its measuring tip placed just at the riser exit or downcomer entrance and 1.083 m from the bottom plate.

Distilled water was used as the continuous phase. The static gas free height h_L of the liquid was varied in the range 1.0–1.3 m, giving draft tube top clearance h_t and bed top clearance h_{Pt} in the range of 0–0.40 m for the range of gas velocities ($U_{gr} = 0.0$–$0.24\ m\ s^{-1}$) used in this study. Different lengths of matrices could be accommodated within the depth of the draft tube. The top end of the packing could be moved up or down to vary the top and bottom clearances of the packing. The effect of the packing height L_p (from 0.6 to 1.0 m) and packing top clearance h_{pt} (from 0.1to 0.4 m) and bottom clearance h_{pb} (from 0.1 to 0.3 m) clearances on the gas holdup and liquid circulation velocity of the ALFBB were studied while maintaining a constant packing porosity $\phi_P = 96\%$ [28] for the cotton fiber and $\phi_P = 96\%$ void volume for the PUF [14,15].

The air/gas flow rate was measured by calibrated rotameter. The local gas holdups in the riser and the downcomer were measured using either a manometer and/or pressure drop [9,11]. The riser and downcomer each had three manometer/pressure taps located at 0.087 m (bottom port), 0.610 m (middle port), and 1.110 m (top port), respectively, from the base plate and were connected to inverted 3-tube type water manometers. For each operating condition, a profile of ε_g versus the height Δz in each region could be drawn according to the following expressions [9,11]:

$$\varepsilon_{r,d} = \left(\frac{\rho_L}{\rho_L - \rho_g}\right)\frac{dh_M}{dz} = \frac{\Delta P_{r,d}}{\rho_L g \Delta z} \tag{1}$$

The overall gas holdup ε_{gT} was determined by visual measurements of the static liquid height h_L and the aerated gas–liquid dispersion height h_D. The gas holdup was calculated from the expression [7,30] were ε_{gr} and ε_{gd} are the riser and downcomer gas holdup, respectively.

$$\varepsilon_{gT} = 1 - \frac{h_L}{h_D} = \frac{A_r\varepsilon_{gr} + A_d\varepsilon_{gd}}{A_d + A_d} \tag{2}$$

The gas holdup in the gas–liquid separator was calculated from a gas volume balance using the following equation [16]:

$$\varepsilon_{gs} = \frac{(\varepsilon_{gT}V_{LT}/1 - \varepsilon_{gT}) - \varepsilon_{gr}H_rA_r - \varepsilon_{gd}H_dA_d}{(V_{LT}/1 - \varepsilon_T) - H_r(A_r - A_d) - h_bA_b} \tag{3}$$

Liquid circulation velocity was determined by a signal-response technique using HCl acid tracer and a pH electrode detector [9,11]. In this work, two pH electrodes, one located at the top in the riser exit and/or downcomer entrance. The second pH electrode was located at the bottom in the riser entrance and/or downcomer exit. The response time of the pH electrodes was 0.1 s. The response of a pulse input of the tracer was signaled by the pH electrodes, and monitored by a pH meter (sensitivity: 0.01), respectively, and then simultaneously recorded every 5 s on a chart and a digital printer. The chart recording was synchronized manually with the introduction of every pulse of 10 mL 4 M (8N) HCL solution through the injection port. For the pH measurements in the riser section, the bottom port was used as the tracer injection port. The top port was used as tracer injection port during pH measurements in the downcomer section. The measured pH values of the liquid in the riser and the downcomer sections were then converted to the actual concentrations through a calibration curve.

The mean circulation time, t_c (time for a liquid volume element to travel once around the riser-downcomer circuit) was determined directly from the response curves observed for each air flow rate and calculated according to the following equation:

$$t_c = \frac{L}{u_L} = \frac{L_r}{u_{L_r}} + \frac{L_d}{u_{L_d}} \tag{4}$$

where L is the mean length of the liquid loop, L_r is the length of the riser section, and L_d is the length of the downcomer section. The number of cycles detectable varied with the airflow rate. At low airflow rate, the number of cycles was six but at the highest airflow rate it was only a few. So experiments carried out at high airflow rates were duplicated to obtain more reliable values for t_c.

With the mean circulation time t_c, the liquid superficial velocities in the riser and downcomer were estimated using the following equations:

$$u_{L_r} = \frac{z_r(1 - \varepsilon_{gr})}{\Delta t_r} \tag{5}$$

$$u_{L_d} = \frac{z_d(1 - \varepsilon_{gd})}{\Delta t_d} \tag{6}$$

where z_r and z_d are the distances between the two pH electrodes in the riser and downcomer, respectively, and Δt_r and Δt_d are the average differences in response time of the second and third peaks of the response curves obtained by the two pH electrodes in the riser and downcomer, respectively. Note that the second and the third peaks of the response curves are used to obtain Δt_r and Δt_d because the first peak of the response curve obtained by the lower pH electrode in the riser is not well-established at higher aeration rate [9,11].

The overall volumetric gas-liquid mass transfer coefficient of oxygen (K_La) was studied using the dynamic "Gas-Out-Gas In" technique [9,11]. The time-change of dissolved (DO_2) tension (%) and concentration in the bulk liquid (C_L) (mg/L) at each position were measured directly using the two YSI Model 05726-24, 19 mm diameter, steam sterilizable polarographic dissolved oxygen electrodes (Cole-Parmer Instrument Co., Jodoin, Anjou, Quebec, Canada), in which the inner boundary layer on the surface of the electrode membrane was quickly established. The dissolved

oxygen electrodes were connected to YSI Model 01971-00 dissolved oxygen meters (Cole-Parmer Instrument Co., Jodoin, Anjou, Quebec, Canada). The two DO_2 electrodes were sampled simultaneously and responses were read with the DO_2 meters and recorded by a chart recorder (Linear, model LR92425 supplied by Barnstead/Thermolyne, Dobuque, Iowa, USA). The mass conservation equation of dissolved oxygen within the boundary layer was written as

$$\frac{\partial C_L(t)}{\partial t} + u_x\frac{\partial C_L(t)}{\partial x} + u_y\frac{\partial C_L(t)}{\partial y} + u_z\frac{\partial C_L(t)}{\partial z} = D_x\frac{\partial^2 C_L(t)}{\partial x^2} + D_y\frac{\partial^2 C_L(t)}{\partial y^2} + D_z\frac{\partial^2 C_L(t)}{\partial z^2} + K_La[C_L^* - C_L] \quad (7a)$$

Based on the assumptions that the liquid phase within the boundary layer was completely mixed, $u_x = u_y = u_z = 0$ and $D_x = D_y = D_z = 0$. Thus, Eq. (7a) was turned into Eq. (7b):

$$\frac{\partial C_L(t)}{\partial t} = K_La[C_L^* - C_L] \quad (7b)$$

where C_L is the bulk concentration of dissolved oxygen and $C_L^*(t)$ is the oxygen concentration in liquid phase at saturation. Upon integration ($C_L(t) = C_{L0}(t = 0)$ and defining a dimensionless dissolved oxygen concentration

$$Z = \frac{C_L(t) - C_{L0}}{C_L^* - C_{L0}} \quad (8)$$

yields:

$$\ln(1 - Z) = -K_La t \quad (9)$$

where C_{L0} is the initial concentration of dissolved oxygen. Thus, the K_La values were obtained by linear regression from the slope of the straight-line of the plot $\ln(1 - Z)$ versus t.

The saturated concentration of dissolved oxygen $C_L^*(t, z)$ depended on temperature and pressure. An equation utilized for estimating the value of C_L^* (in parts per million) was written as

$$C_L^*(t, z) = \frac{yP_t\rho_L M_{O_2} + y\rho_L^2 g(1 - \varepsilon_{gT})(h_D - \Delta z)M_{O_2}}{HM_{H_2O}} \quad (10)$$

where P_t is the pressure at the top of the bioreactor, g is the gravitational acceleration, and h_D the height of the liquid dispersion, ε_{gT} is the total (overall) fractional gas holdup, and y is the molar fraction of oxygen in the gas phase [31]. The Henry's constant H for water as a function of temperature is given by the following relationship [8]

$$H \times 10^9(Pa) = 2.211 + 0.496T \quad (11)$$

All the values of the volumetric mass transfer coefficient (K_La) obtained were corrected for temperature. Hence, the mass transfer coefficient at 20 °C was evaluated using the following equation [1,11,31]:

$$K_La(20) = K_La(T)[1.0125]^{T-20} \quad (12)$$

where $K_La(20)$ and $K_La(T)$ are the mass transfer coefficients at 20 °C and at the experimental temperature, respectively. All the data presented here were converted to 20 °C.

3. Results and discussion

3.1. Gas holdup

3.1.1. Effect of packing nature, length, and bed top clearance on gas holdup

The hydrodynamic and mass transfer studies were contacted in a closed internal loop airlift bioreactor with or without fibrous-bed packing. The gas holdup values obtained in this study are shown in Figs. 2 and 3 for various matrices at different packing heights and bed top and bottom clearances. For the range of superficial gas velocity examined, churn (or slug) turbulent flow patterns, which are characterized by large bubbles moving at high rise velocities in the presence of small bubbles were observed in the ALB without packing at low gas velocities $U_{gr} \leq 0.08\ m\ s^{-1}$. An increase of the gas velocity changed the flow pattern from churn turbulent to bubble-flow regime, where the gas was dispersed into small bubbles with narrow size distribution, which began to be entrained into the downcomer. The transition from churn turbulent to bubble-flow regime in the packing occurs at a higher gas velocity in comparison with the ALB without packing. In the latter case, the churn turbulent regime starts at approximately $0.08\ m\ s^{-1}$. Bhatia et al. [32]

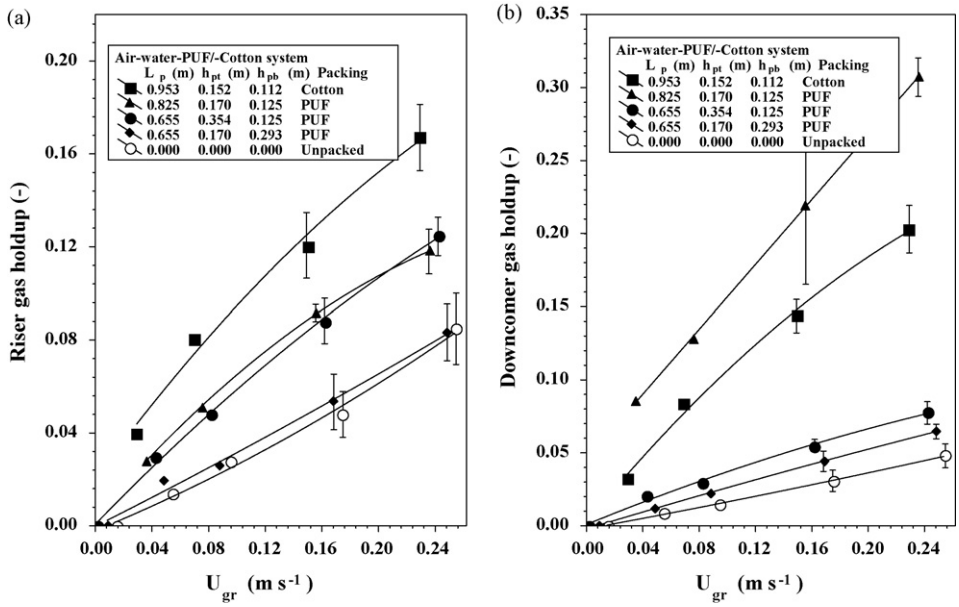

Fig. 2. Effect of packing nature, packing height, and bed clearances on (a) riser and (b) downcomer gas holdup in the ILALB with and without packing (h_L = 1.208 m, $L_{r/d}$ = 1.02 m, h_t = 0.114 m, h_b = 0.064 m, h_{pb} = 0.112 m, m_p = 0.004 m).

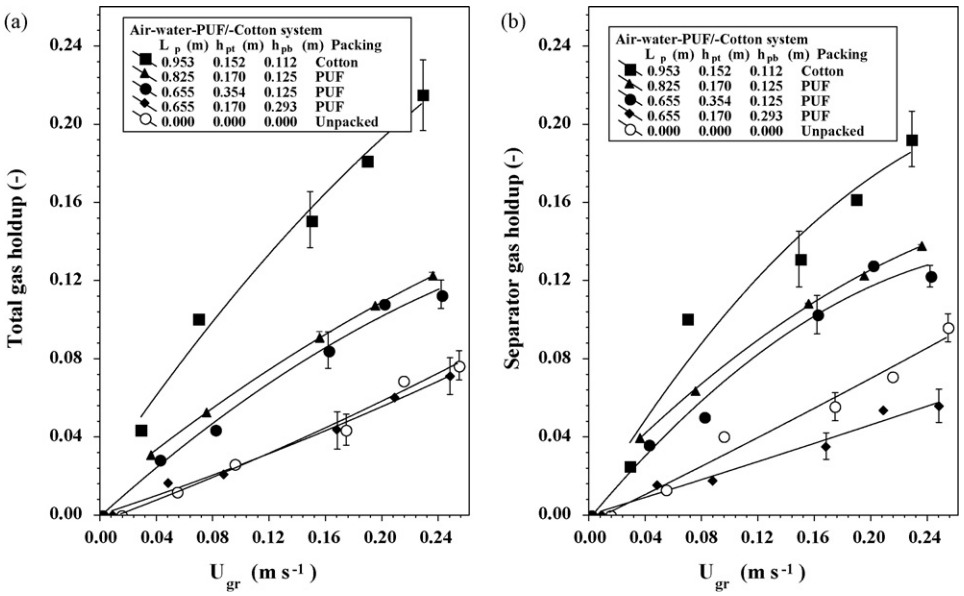

Fig. 3. Effect of packing nature, packing height, and bed clearances on (a) total and (b) separator gas holdup in the ILALB with and without packing (h_L = 1.208 m, $L_{r/d}$ = 1.02 m, h_t = 0.114 m, h_b = 0.064 m, h_{pb} = 0.112 m, m_p = 0.004 m).

and Moustiri et al. [33] have shown that the packing causes bubble breakup and that there is no formation of large bubble especially in the packed downcomer, unlike in the riser region and unpacked airlift column operating in the churn turbulent regime. The presence of fibrous packing prevents small bubble disengagement from the gas–liquid separator even at higher gas velocity of 0.24 m s^{-1} and enhances the gas holdup value at the expense of decreased bubble coalescence [11,34,35]. It is interesting to note in Fig. 12 that within the range of superficial gas velocities tested, an increase in liquid circulation velocity involves a slight decrease in gas holdup. This is more evident in the riser region than in the downcomer region where gas holdup is much higher than in the former.

A large difference in the gas holdup values is observed with and without fibrous-bed packing at high values of superficial gas velocity, thus making the fibrous packing more efficient in this range of operation. Enhanced gas holdup may be attributed to reduced bubble size and liquid circulation velocity. The former is associated with the cutting and shearing of the bubbles by the packing [32,33], while the latter is attributed to a drop in the interstitial gas velocity owing to the increased resistance in the packed downcomer [23]. The solid fraction occupied by the fibrous-bed packing is very low (i.e., $\phi_p \approx 0.96$ for cotton and 0.96 for PUF) and enables high liquid phase volumes with high gas velocity to be used, the corresponding pressure drop created being low.

Nevertheless, high gas holdup was observed with large cotton packing than with PUF. In the present study using cotton packing height of L_p = 0.953 m, an improvement factor of 5.77 (∼70% increase) was observed for the downcomer gas holdup (ε_{gd}: 0.039–0.225), which was 4.06 times higher than that using PUF packing height of L_p = 0.825 m and 5.02 higher than using PUF packing height of L_p = 0.655 m. At the same time, an improvement factor of 2.25 (∼39% increase) was also observed for the riser holdup (ε_{gr}: 0.063–0.142) using cotton packing of height L_p = 0.953 m, which was 1.58 times higher than that using PUF packing height of L_p = 0.825 m and 1.96 higher than using PUF packing length of L_p = 0.655 m as shown in Fig. 4a and b. It is also interesting to note that, the gas holdups observed using PUF packing height of L_p = 0.825 m (h_{pt} = 0.170 m, h_{pb} = 0.125 m) and L_p = 0.655 m (h_{pt} = 0.354 m, h_{pb} = 0.125 m) are essentially identical (cf. Figs. 4a, 5a and b), indicating the balancing of the decrease in ε_{gr} by an increase of ε_{gd}, and thus an increase in the liquid circulation velocity.

An improvement factor of 3.04 (∼51% increase) was also observed for total gas holdup (ε_{gT}: 0.0497–0.1512) of the unpacked ALB with a cotton packing height of L_p 0.953 m, which was 1.72 times higher than that with PUF packing height of L_p 0.825 m and 1.83 times than with PUF packing height of L_p 0.655 m as shown in Fig. 3a. Similarly, an improvement factor of 2.19 (∼37% increase) was also observed for the separator gas holdup (ε_{gS}: 0.0609–0.1334) with cotton packing height of L_p 0.953 m, which was 1.30 times higher than that with PUF packing height of L_p 0.825 m and 1.40 times than with PUF packing height of L_p 0.655 m, thus making cotton packing more efficient. These observations, however, tend to deviate from other studies [36,37]. It is also worthy to note that, the separator and total gas holdups measured with PUF packing length of L_p = 0.825 m (h_{pt} = 0.170 m, h_{pb} = 0.125 m) and L_p = 0.655 m (h_{pt} = 0.354 m, h_{pb} = 0.125 m) PUF bed generally behaves in the same way. Furthermore, the riser and total gas holdup data observed in Fig. 4a and Fig. 3a with PUF packing length of L_p = 0.655 m with small top (h_{pt} = 0.170 m) and large bottom (h_{pb} = 0.293 m) clearances, were essentially identical to data in ILALB without packing. But, gas holdup data measured using packing with large top (h_{pt} = 0.354 m) and small bottom (h_{pb} = 0.125 m) clearances were two times higher than similar packing with small top (h_{pt} = 0.170 m) and large bottom (h_{pb} = 0.293 m) clearances. These observations also tend to be in agreement with those reported by Su and Heindel [37], who found that the gas holdup in shorter nylon fiber packing was no different from that of the longer fiber.

The high gas holdup observed using long cotton packing was due to increased shearing forces and decreased bubble coalescence. The former is associated with the stiffness of the cotton fiber surface and the later was due to the wettable cotton fiber surface, which tends to act, as a buffer between two adjacent gas bubbles [38]. In contrast, the hydrophobic nature of the PUF surface tends to promote bubble coalescence by enhancing film rupture when two bubbles approach, leading to a low gas holdup.

It also appears from Fig. 2 that gas holdup is a function of superficial gas velocity according to the empirical correlation previously

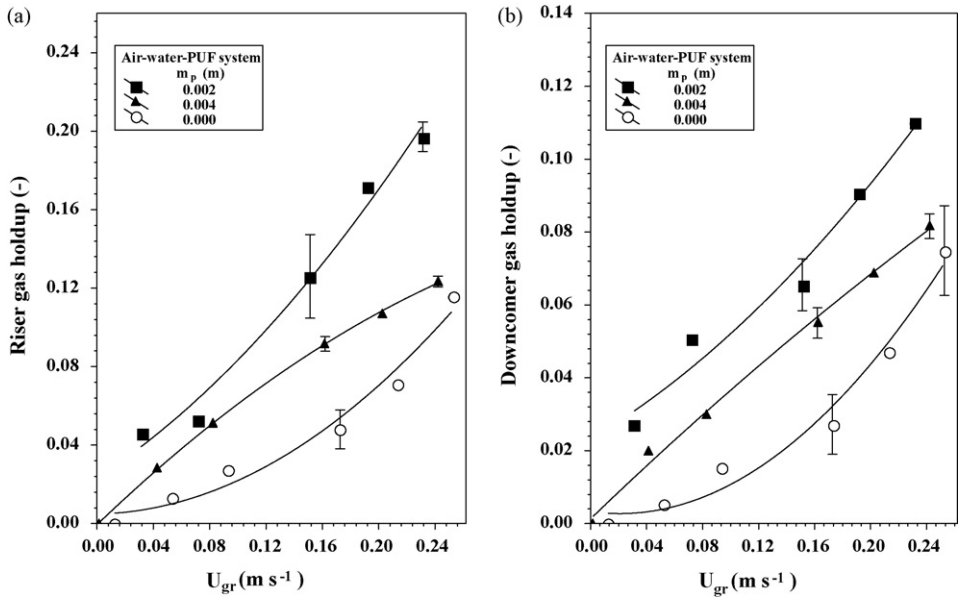

Fig. 4. Effect of gap width m_p between adjacent fiber surfaces on (a) riser and (b) downcomer gas holdup, respectively, in the ILALB with polyurethane foam (PUF) packing (h_L = 1.145 m, $L_{r/d}$ = 1.02 m, h_t = 0.115 m, h_b = 0.06 m, L_p = 0.825 m, h_{pt} = 0.170 m, h_{pb} = 0.125 m).

reported by Nikakhatari and Hill [23]:

$$\varepsilon_{gr} = \alpha U_{gr}^{\beta} \quad (13a)$$

Fitting Eq. (13a) to experimental data for the riser and downcomer gas holdups for both cotton and polyurethane foam packing, the parameters determined by multiple regression are:

$$\alpha{=}1.002;\ \beta{=}1.319,\ R{=}0.963;\ R^2 = 0.928 \ldots \text{cotton packed bed} \quad (13b)$$

$$\alpha = 0.561;\ \beta = 0.934,\ R = 0.899;\ R^2 = 0.808 \ldots \text{PUF packed bed} \quad (13c)$$

A linear correlation with α = 0.499 and β = 1 was also found for the case of unpacked (control) ALB with correlation coefficient: R = 0.835 and R^2 = 0.697. The gas holdup measurements revealed that the downcomer gas holdup is a linear function of the riser gas holdup according to the correlations

$$\varepsilon_{gd} = 1.401\varepsilon_{gr},\ R = 0.982;\ R^2 = 0.965;\ \text{S.E.} = 0.016 \ldots \text{cotton packed bed} \quad (14a)$$

$$\varepsilon_{gd} = 0.649\varepsilon_{gr},\ R = 0.996;\ R^2 = 0.991;\ \text{S.E.} = 0.002 \ldots \text{PUF packed bed} \quad (14b)$$

$$\varepsilon_{gd} = 0.672\varepsilon_{gr},\ R = 0.986;\ R^2 = 0.972;\ \text{S.E.} = 0.003 \ldots \text{Control(unpacked bed)} \quad (14c)$$

which were found to fit the gas holdup data for the packed downcomer and control (unpacked).

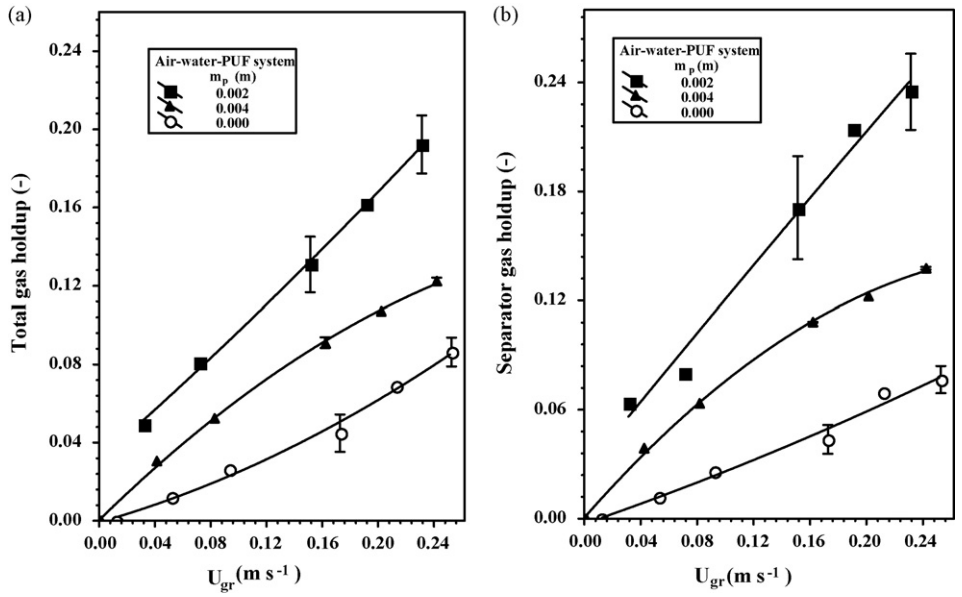

Fig. 5. Effect of gap width m_p between adjacent fiber surfaces on (a) total and (b) separator gas holdup, respectively, in the ILALB with polyurethane foam (PUF) packing (h_L = 1.145 m, $L_{r/d}$ = 1.02 m, h_t = 0.115 m, h_b = 0.06 m, L_p = 0.825 m, h_{pt} = 0.170 m, h_{pb} = 0.125 m).

3.1.2. Effect of gap width between adjacent fiber surfaces (m_p) on gas holdup

In Figs. 4 and 5, the gas holdup values measured using a PUF packing bed are presented as a function of the superficial gas velocity U_{gr} for different gap width m_p between the adjacent fiber surfaces. As shown in Fig. 4, packing with gap width of m_p = 0.002 m between adjacent fiber surfaces improved the riser gas holdup (ε_{gr}: 0.0686–0.1138) and downcomer gas holdup (ε_{gd}: 0.0388–0.0639) of the unpacked ILALB by a factor of 1.66 (~25% increase). In the case of the riser gas holdup, this factor was 1.3 times higher. But, for the case of downcomer gas holdup it was 0.72 times lower than with m_p = 0.004 m as shown in Fig. 4.

Similarly, an improvement factor of 2.53 (~43% increase) was also observed for the total gas holdup (ε_{gT}: 0.0531–0.1341) with a gap width of m_p = 0.002 m, which was 1.52 times higher than that with C_p = 0.004 m as shown in Fig. 5. At the same time, an improvement factor of 3.34 (ε_{gS}: 0.0497–0.1673) was observed for the separator gas holdup with a gap width of m_p = 0.002 m, which also was 1.64 times higher than that with m_p = 0.004 m, thus m_p = 0.002 m the more effective gap width between fiber surfaces.

A small gap width between fiber surfaces promotes bubble coalesce [39] and higher pressured drop [40] leading to a reduced liquid circulation velocity in the packing zone. In such situation, some of the gas bubbles disengage in the gas–liquid separator. This is evident in the downcomer gas holdup being lower than that in the riser. The re-dispersion of the gas bubbles at large spacing distance (m_p = 0.004 m) was not so effective, because of the decreased pressured drop and increased free flow area [40] at which decreased coalescence is expected, leading to low gas holdup.

In general term, the separator gas holdup behaves in the same manner as the total gas holdup. The enhanced gas holdup contributes to an increase in interfacial area, leading to an increase in the mass transfer coefficient.

3.2. Liquid circulation velocity

3.2.1. Effect of packing nature and height on liquid circulation velocity

In Fig. 6, the liquid circulation velocity in the riser and downcomer regions is presented as a function of the superficial gas velocity for different matrices of various lengths. A large difference in the liquid circulation velocity value is observed with and without packing at high values of the superficial gas velocity. Using the fibrous-bed in the ALB, in spite of the high packing porosity, resulted in a large decrease in liquid circulation velocity. The packing height has also a dramatic effect on the liquid velocity in the ALFBB. A cotton packing of length L_p = 0.953 m (h_{pt} = 0.152 m, h_{pb} = 0.112 m) decreases the riser liquid velocity U_{Lr} from 0.2158 to 0.1591 m s^{-1} (i.e., 26.3% decrease) and downcomer liquid velocity from 0.2298 to 0.1595 m s (i.e., 30.6% decrease). Similarly, a PUF packing of length L_p = 0.825 m (h_{pt} = 0.170 m, h_{pb} = 0.125 m) decreases the riser liquid velocity U_{Lr} to 0.1787 m s^{-1} (i.e., 17.2% decrease) and downcomer liquid velocity to 0.1881 m s (i.e., 18.2% decrease). A short PUF packing length L_p = 0.655 m (h_{pt} = 0.170 m, h_{pb} = 0.293 m), however, decreased the riser liquid velocity to only 0.0972 m s (i.e., 55.1%), and no appreciable drop in the downcomer liquid velocity. Slightly higher (~1.4 times) decrease in the riser liquid velocity (0.2158–0.1370 m s^{-1}; i.e., 36.5%) was observed also using short packing length of L_p = 0.655 m with large top clearance of h_{pt} = 0.354 m (h_{pb} = 0.125 m). It is clear from these results that the bed top clearance exerts more influence on the liquid circulation velocity than the bottom clearance. Increasing the top and bottom clearances of the bed reduces reversal flow resistance above and below the packed bed. Thus, the increased surface area A_p and the tortuosity of the packing material caused by greater packing height L_p from 0.6 to 1.0 m or by increased top bed clearance h_{pt} from 0.170 to 0.354 m causes the frictional flow resistance, thereby slowing down the liquid circulation velocity over the tested superficial gas velocity range from 0 to 0.24 m s^{-1}. The decrease in liquid velocity promotes higher gas holdups since the bubble rising velocity has been enhanced.

3.2.2. Effect of gap width between fiber surfaces on liquid circulation velocity

Fig. 7 shows the effect of gap width m_p, between adjacent fiber surfaces on riser and downcomer liquid circulation velocities for the air–water system studied with polyurethane foam (PUF) as the fibrous matrix. As seen from this figure, the liquid velocities at m_p = 0.002 m are slightly lower than those at m_p = 0.004 m under similar conditions. For smaller spacing distance between adjacent fiber surfaces, the liquid velocity is restricted by the high-pressure drop in the packed zone that some of the kinetic energy (K.E.) of

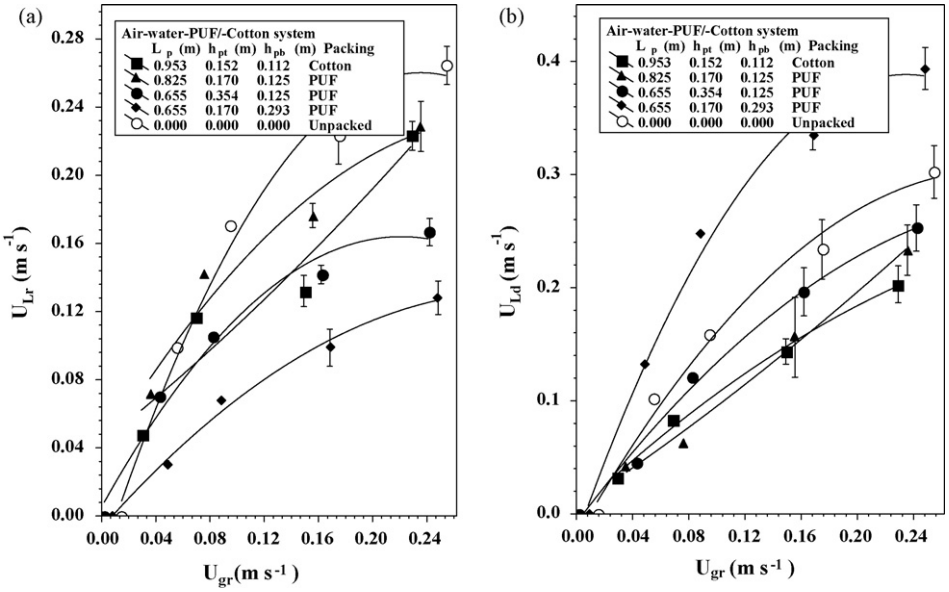

Fig. 6. Effect of packing nature, packing height, and bed clearances on liquid circulation velocities in the ILALB with and without packing (h_L = 1.145 m, $L_{r/d}$ = 1.02 m, h_t = 0.156 m, h_b = 0.06 m, h_{pb} = 0.125 m). (a) Riser and (b) downcomer liquid velocities, respectively.

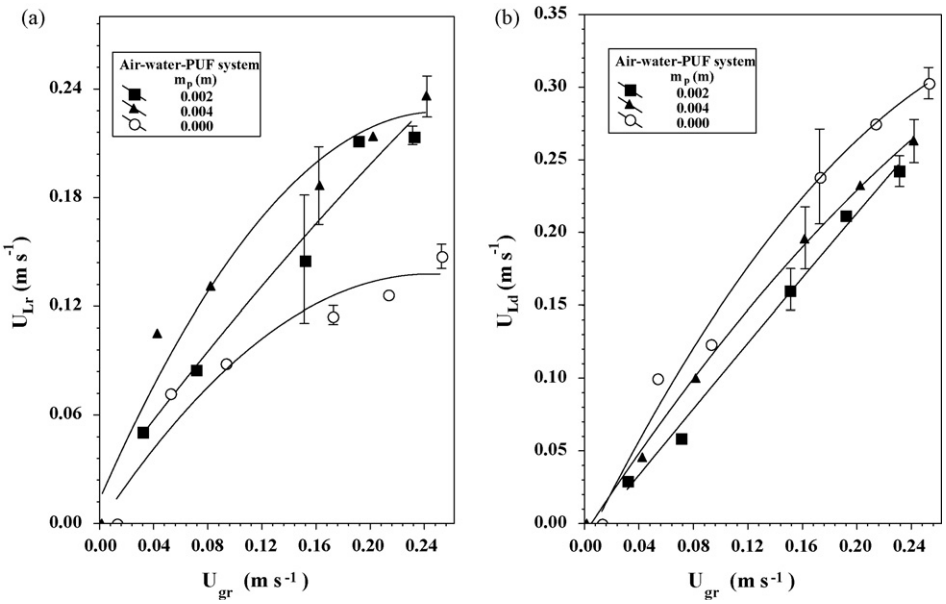

Fig. 7. Effect of gap width m_p between adjacent fiber surfaces on liquid circulation velocity in the ILALB with and without polyurethane foam (PUF) packing (h_L = 1.145 m, $L_{r/d}$ = 1.02 m, h_t = 0.115 m, h_b = 0.06 m, L_p = 0.825 m, h_{pt} = 0.170 m, h_{pb} = 0.125 m). (a) Riser and (b) downcomer liquid circulation velocities, respectively.

the flowing liquid is spend in overcoming frictional resistance in the packing zone.

In general, the liquid velocities in the unpacked system (m_p = 0.000 m) is much higher than packing systems with either m_p = 0.002 m or 0.004 m due to the flow resistance in the packing. Packing with narrow gaps (m_p = 0.002 m) between adjacent fiber surfaces decreased the riser and downcomer liquid velocities in the unpacked ILALB from 0.226 m s^{-1} to ~0.138 m s^{-1} (i.e., ~24%). In contrast, packing with large gaps between fiber surfaces (m_p = 0.004 m) decreases the riser and downcomer liquid velocities of the unpacked ALB only from 0.226 to 0.175 m s^{-1} (i.e., ~13%) and 0.160 m s^{-1} (i.e., ~17%), respectively.

In airlift bioreactors, liquid circulation velocity is a factor of frictional energy losses as the fluid circulates through the loop. Therefore, it is anticipated that different values will occur due to slight changes in the geometrical design of the ILAB [9,11]. Nikakhtari and Hill [24] also observed a dramatic reduction in U_{Lr} from 0.32 to 0.07 m s^{-1} in the presence of packing (in their case, 1.2 m long bed of stainless steel mesh and porosity of 0.99) in external loop airlift bioreactor (ELALB). Meng et al. [36] also observed reduction in U_{Lr} from 0.19 to 0.10 m s^{-1} in the presence of woven nylon packing (porosity: 0.9 to 1.0) as the height of the packed bed in an ELALB increased from 0 to 0.80 m, which was less than observed by Nikakhtari and Hill [24]. In a similar related work, Chisti and Moo-Young [21] also observed a reduction in the liquid velocity in the presence of packing (in their case, 1.0 m deep bed of spheres with a diameter of 0.01 m and porosity of 0.4) in an ELALB, which was more than that observed by either Nikakhtari and Hill [24] or Meng et al. [36]. The liquid reduction observed in these earlier studies using fibrous packing in an ELAB is more than that observed in the present study using fibrous packing in an ILALB. All the experimental data indicates that disengagement was a much more effect in this bioreactor design. This shows that the cross-sectional area of the gas-liquid separator has a strong influence on the fluid dynamics of the bioreactor. This was shown by a regression analysis, which is presented in the preceding sections.

3.3. Mass transfer

In the dynamic measurement of K_La, the assumption regarding the state of mixedness in the bioreactor can influence the K_La value [3]. The validity of Eqs. (4) and (6) used to calculate the K_La was based on the assumption that there is perfect mixing of the liquid phase in the bioreactor. The assumed perfectly mixed state was approached closely, as confirmed in Fig. 8 where, for any given superficial gas velocity the K_La values obtained with the dissolved oxygen probes located to the top and bottom of the bioreactor showed a fairly mutual agreement, generally within 12% of the mean value for the two locations. Mixing was fairly good at all gas velocities in the ILALB. This is reflected in Fig. 8, where the difference between the top and bottom K_La values is generally small. For the case of ILALB with packing, both probes displayed almost similar behavior. The K_La increased with superficial gas velocity, reaching a maximum value at 0.18 m s^{-1}. This K_La value start to decline at gas velocities >0.18 m s^{-1}. In contrast, the K_La values measured in the ILALB without packing were comparatively low, and increased linearly with superficial gas velocity, especially at gas velocities U_{gr} > 0.15 m s^{-1}. In either case, lower K_La values were observed with the bottom probe, especially at low superficial gas velocities. The maximum difference between the probes accounted only 0–12% in the ILALB with packing and 0–24% in ILALB without packing. It was, therefore, decided to treat the data obtained from top probe, as the representative of the mass transfer in the ILALB.

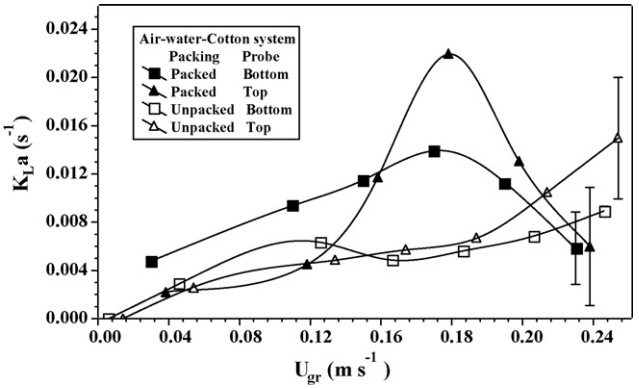

Fig. 8. Effect of dissolved oxygen probe location on mass transfer coefficient K_La in the ILALB, (a) without packing and (b) with cotton packing (h_L = 1.245 m, $L_{r/d}$ = 1.024 m, L_p = 0.953 m, h_{pt} = 0.191 m, h_{pb} = 0.112 m, h_t = 0.156 m, h_b = 0.064 m).

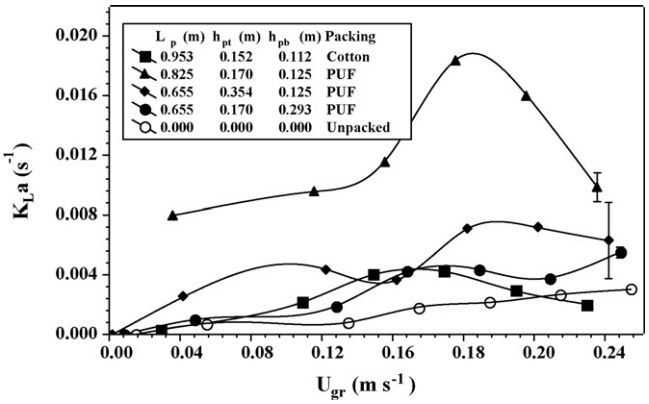

Fig. 9. Effect of packing nature, height, and bed clearances on mass transfer coefficient K_La in the ILALB with and without packing (h_L = 1.208 m, $L_{r/d}$ = 1.024 m, h_t = 0.156 m, h_b = 0.064 m). (a) Large packing, (b) small packing.

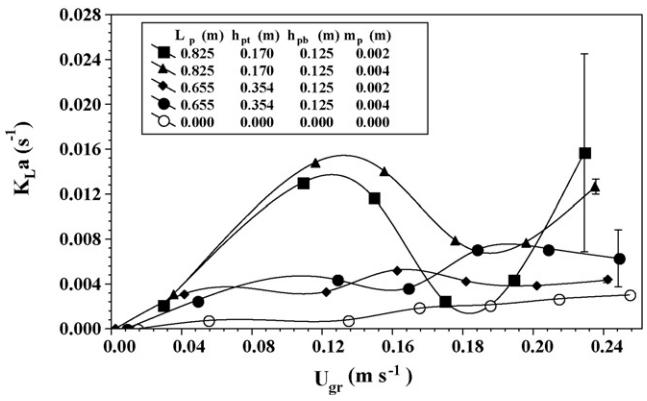

Fig. 10. Effect of gap width m_p between adjacent fiber surfaces on K_La in ILALB with and without polyurethane foam (PUF) packing (h_L = 1.145 m, $L_{r/d}$ = 1.02 m, h_t = 0.115 m, h_b = 0.06 m, h_{pb} = 0.125 m). (a) L_p = 0.825 m, h_{pt} = 0.170 m; (b) L_p = 0.655 m, h_{pt} = 0.354 m.

The liquid mixing time of 12–31 s and 16–32 s was observed in the downcomer and riser, respectively of an ILALB with cotton packing, which were $\leq 1/K_La$, and therefore, the electrode response delays could be neglected in the calculation of K_La [24].

3.3.1. Effect of packing nature, height L_p, and bed top clearance on mass transfer coefficient K_La

Fig. 9 shows mass transfer coefficient for the air-water system in the ILALB with and without the fibrous-bed. The K_La increases to a maximum value up to a gas velocity U_{gr} = 0.142 m s^{-1}, and thereafter decreases with increasing gas velocity due to the transition from bubbly flow regime (U_{gr} < 0.142 m s^{-1}, characterized by almost uniformly sized bubbles) to churn turbulent flow (U_{gr} > 0.142 m s^{-1}) which is accompanied by formation of large bubbles with small interfacial area.

A large difference in the average K_La values in the case without and with packing (1.2–2.2 times) were observed. A similar difference in K_La values with cotton and PUF packing was also observed. At the same time, the maximum K_La (K_La = 0.00726 s^{-1}) value measured using PUF packing height of L_p = 0.825 m (h_{pt} = 0.170 m, h_{pb} = 0.125 m) was 1.7 times higher than K_La (0.00422 s^{-1}) value observed in cotton packing height of L_p = 0.953 m (h_{pt} = 0.152 m, h_{pb} = 0.112 m) and ~2 times than the K_La (0.00363 s^{-1}) value observed in PUF packing height of L_p = 0.655 m (h_{pt} = 0.354 m, h_{pb} = 0.125 m), and 2.3 higher than in unpacked ILALB. It is also interesting to note that the K_La value (0.00264 s^{-1}) observed using PUF packing height of L_p = 0.655 m with small top (h_{pt} = 0.170 m) and large bottom (h_{pb} = 0.293 m) clearances, was ~1.4 times lower than the value in a similar packing height with large top (h_{pt} = 0.354 m) and small bottom (h_{pb} = 0.125 m) clearance, but 1.2 times higher than in ILALB without packing.

ThE increased K_La observed in Fig. 9 must be due to increased interfacial area associated with bubble breakup [40]. An additional increase in K_La is expected in the fibrous-bed bioreactor system proposed in this study, due to enhanced K_L value by increased number of localized turbulent eddies in the packing.

3.3.2. Effect of gap width m_p between fiber surfaces on mass transfer coefficient K_La

Fig. 10 shows some K_La values measured in the air–water system with and without the fibrous-bed. An influence of the fibrous-bed structure on the K_La value was observed for a small gap width between fiber surfaces (m_p = 0.002 m). Large packing height coupled with small gap width m_p = 0.002 m, increases the K_La value of the conventional ILALB from 0.0034 s^{-1} to 0.0088 s^{-1} (~2.6 times higher than that in conventional ILALB) or (~44% increase) due to increased total gas holdup (ε_{gT}) and improved gas–liquid interfacial area (cf. Fig. 10). Increasing the gap width between fiber surfaces decreases the pressure drop but also decreases the K_La value. Therefore, m_p = 0.004 m increases the K_La value to 0.0068 s^{-1}, which 1.3 times lower than that with m_p = 0.002 m, but 2 times higher (~33% increase) than that in conventional ALB. Therefore, proper design of the gap width between fiber surfaces may increase oxygen mass transfer and also provide other advantages such as reduced pressure drop and less bioreactor plugging potential.

In general, K_La value observed in the ILALB with packing is always higher than the K_La value in the unpacked ILALB. In earlier studies, Nikakhtari and Hill [23] observed increased K_La value from 0.0011 s^{-1} (unpacked) to 0.0042 s^{-1} in an external loop airlift bioreactor (ELALB) packed with nylon mesh (L_p = 1.09 m, ϕ_p = 0.963) which is 1.73 times lower than the K_La value observed using PUF packing and essentially equal to the K_La value observed using cotton packing in the present study. However, the K_La value observed by Nikakhtari and Hill [24] in an external loop airlift bioreactor (ELALB) packed with stainless steel mesh (L_p = 1.2 m, ϕ_p = 0.99) and operated at high gas velocity was about 3 times that obtained using PUF packing (L_p = 0.825 m, ϕ_p = 0.96) and 5 times higher that using cotton packing (L_p = 0.953 m, ϕ_p = 0.93) in the present study. Recently, Martinov et al. [25] also observed increased K_La value from 0.01 s^{-1} (unpacked) to 0.026 s^{-1} in a laboratory-scale glass column with recycling packed with PEVA fibrous-bed (L_p = 0.26 m), which was about 3.6 times that obtained using PUF packing (L_p = 0.825 m, ϕ_p = 0.96) and 6.2 times higher that using cotton packing (L_p = 0.953 m, ϕ_p = 0.93) also in the present study. Okada et al. [22] also observed enhanced K_La value from 0.015 s^{-1} (unpacked) to 0.035 s^{-1} in an external loop airlift bioreactor (ELALB) packed with 15 mm steel pall ring (L_p = 0–0.4 m), which was about 4.8 times that obtained using PUF packing (L_p = 0.825 m, ϕ_p = 0.96) and 8.3 times higher than that using cotton packing (L_p = 0.953 m, ϕ_p = 0.93) examined in the present study. Similar studies using packing materials used in biofilters and biotrickling filters to improve K_La value were reported by Kim and Deshusses [41]. The data obtained for K_La with different fibrous packing and range of packing heights, bed clearances, and gap width between fiber surfaces studied in this work could be correlated as showing the next section.

4. Correlation of experimental results

4.1. Gas holdup

It is believed that packing causes changes in the gas holdup due to greater flow tortuosity and therefore longer path lengths

for bubbles to travel. Impacts between bubbles and with the packing material can greatly alter hydrodynamics, including gas holdup. Over the range of packing height and top and bottom clearances used in this investigation, these features seem to be directly related to the amount of packing because the gas holdup tend to increase with increases in packing height, bed top and bottom clearances and a decrease in the gap between fiber surface as shown in Figs. 4–6. The increase of gas holdup with the packing height, top and bottom bed clearances, and fiber surface spacing could be accurately modeled by a modified equation of the form described earlier by Kilonzo et al. [9,11] for gas holdups in an internal loop airlift reactors. On the basis of their information, the following correlations were obtained from 56 data points to predict the gas holdup for each hydrodynamic region of the ALR proposed in this study.

Correlation ($R = 0.998$; $R^2 = 0.996$; SD = 0.075; S.E. = 0.0078) for riser gas holdup ε_{gr}:

$$\varepsilon_{gr} = 2.59\left(\frac{U_{gr}}{\sqrt{gd_c}}\right)^{0.78}\left(\frac{h_{pb}}{d_d}\right)^{-0.39}\left(\frac{d_S}{4d_c}\right)^{-0.06} \times \left(\frac{m_p}{d_d}\right)^{0.82}\left(\frac{L_p}{d_c}\right)^{-0.33}\left(\frac{h_{pt}}{d_d}\right)^{-0.18} \quad (15)$$

Correlation ($R = 0.952$; $R^2 = 0.888$; SD = 0.051; S.E. = 0.0037) for downcomer gas holdup ε_{gd}:

$$\varepsilon_{gd} = 3.96\left(\frac{U_{gr}}{\sqrt{gd_c}}\right)^{0.97}\left(\frac{h_{pb}}{d_d}\right)^{0.77}\left(\frac{L_p}{d_c}\right)^{-0.26}\left(\frac{m_p}{d_d}\right)^{-0.31} \times \left(\frac{d_S}{4d_c}\right)^{-3.8}\left(\frac{g\rho_L^2 d_c^3}{\mu_L^2}\right)^{-0.13} \quad (16)$$

Eqs. (15) and (16) can be used to predict the riser, downcomer, total or separator gas holdups, respectively, when the packing is present in the downcomer. They are valid over range of variables (Eq. (17)) used in this study.

$$\left.\begin{array}{l} 0.6 \le L_P \le 1.0m \\ 0.0 \le h_{Pt} \le 0.4m \\ 0.1 \le h_{Pb} \le 0.4m \\ 0.002 \le m_P \le 0.006m \\ 0.0 \le U_{gr} \le 0.24m/s \end{array}\right\} \quad (17)$$

Correlations 15 and 16 reveals the roles played by the different regions in the internal loop airlift bioreactor (ILALB) with packing. The relative contributions of riser and downcomer to the total holdup are different and complementary. The main term $(U_{gr})/(gd_c)^{0.5}$ represents here the influence of gas-input rate, and so energy input rate. It affects the holdup much more strongly in the riser than in the downcomer, and the balance between them gives an exponent of almost for the total holdup. The ratio h_{pb}/d_d, represents the bottom clearance of the bed, and exerts its influence on the gas holdup in all the regions. The exponent of (h_{pb}/d_d) is negative in the correlation of holdup in the downcomer, indicating that as h_{Pb} increases ε_{gd} decreases. As mentioned earlier, this can be due to the effect of the flow constriction in the liquid velocity. In the riser, however, the exponent is positive and quite large, indicating the effect of the liquid velocity. As the h_{Pb} increases, the liquid circulation increases as well, and more gas bubbles are carried over into the downcomer. The exponent 0.77 on (h_{Pb}/d_d) in Eq. (16) indicates that ε_{gd} could be increased up to 4 times by changing the bottom clearance within the range of variables tested here.

The effect of the bed top clearance, represented by the ratio (h_{pt}/d_d), had a modest influence on the riser holdup, but not the downcomer holdup. An increase in the bed top clearance diminishes the gas holdup, as indicated by the negative exponent. The correlations show that the viscosity, at least for the liquid tested and within the range of the variables inspected, does not have a statistically significant influence on either downcomer holdup or riser holdup, because it was kept constant. In consequence, the dimensionless group $(g\rho_L^2 d_c^3)/(\mu_L^2)$ does not show a statistically significant influence on gas holdup investigated in this study. The width gap between adjacent fiber surfaces, represented by the ratio (m_p/d_d), exerts strong influence on the downcomer gas holdup than on riser gas holdup. The exponent of (m_p/d_d), is negative in the correlation of holdup in the downcomer, indicating that as m_p increases ε_{gd} decreases. This can be seen as the effect of shear thinning of the packing on gas bubbles.

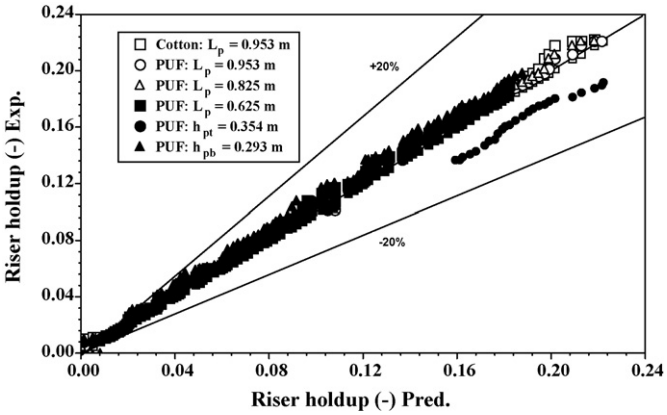

Fig. 11. Parity plot comparing the predicted riser gas holdup calculated using Eq. (15) to the data measured in the ILALB with packing.

Figs. 11 and 12 compares the values of the gas holdup calculated using Eqs. (15) and (16) with experimental data. Good agreement was found with a deviation of ±21% for the riser and ±20% for the downcomer, which means Eqs. (15) and (16) satisfactorily, fits the experimental data in the present study.

4.2. Correlation for liquid circulation

Based on the energy balance over the airlift circulation loop, the driving force for the liquid circulation in the bioreactor is produced by the change in energy as gas bubbles rise and expand up the riser. The energy balance over the loop in the bioreactor shown in Fig. 2 is written as:

$$E_i = E_r + E_d + E_B + E_T + E_f + E_P \quad (18)$$

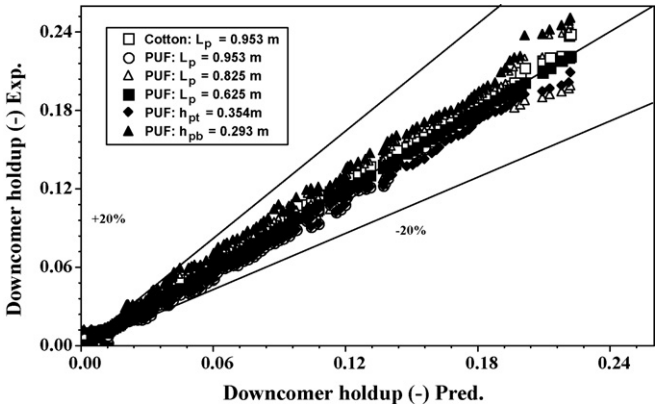

Fig. 12. Parity plot comparing the predicted downcomer gas holdup calculated using Eq. (16) to the data measured in the ILALB with packing.

in which E_b, energy dissipation due to fluid turnaround at the bottom (W); E_d, energy dissipation rate due to gas in the downcomer (W); E_f, energy dissipation due to wall-friction (W); E_i, energy input rate (W); E_p, energy dissipation rate in the packed fibrous-bed (W); E_r, energy dissipation due to bubble rise in the riser (W); E_t, energy dissipation due to fluid turnaround at the top (W). The energy input due to isothermal gas expansion in the riser (E_i) is given by:

$$E_i = QP_h\left(1 + \frac{\rho_D g h_D}{P_h}\right) \tag{19}$$

4.2.1. In the riser

The energy dissipation due to wakes behind bubbles in the riser (E_r) can be obtained by energy balance on the riser as the control volume assuming that $\rho_L \gg \rho_g$:

$$E_r = E_i - \rho_L g h_D U_{Lr} A_r \varepsilon_{gr} \tag{20}$$

4.2.2. In the top and bottom section

The liquid velocity $U_{L,avmt}$, which considers the liquid defection in the top due to its contraction in the downcomer and separator gas holdup was evaluated according to a modified method described by Kochbech and Hempel [42]. Similarly, the liquid velocity $U_{L,avmb}$, which considers also the liquid deflection in the bottom due its expansion in the riser, was evaluated using similar procedure Kochbech and Hempel [42]. Thus, the energy dissipation due to contraction, expansion, and reversal of the fluid flow in the top (E_t) and turn around at the bottom (E_b) sections of the proposed bioreactor is given by:

$$E_b + E_t = \frac{1}{2}\rho_L\left\{\frac{U_{Ld}^3 A_d^3 f_b}{\{A_d + (A_r - A_d)[1-(\varepsilon_{gr}+\varepsilon_{gd})]\}^2} + \frac{U_{Lr}^3 A_r^3}{(1-\varepsilon_{gr})^2} f_{tE} + \frac{U_{Ld}^3 A_d^3 f_{tC}}{[1-(\varepsilon_{gs}+\varepsilon_{gr})]^2}\right\} \tag{21}$$

where f_{tE}, f_{tC}, and f_b are the loss coefficients due to fluid expansion and contraction at the top and expansion in the bottom, respectively. ε_{gs} is the disengagement zone (separator) gas holdup.

Because of the continuity relationship for incompressible flow governs the flow between the riser and the downcomer, we have

$$U_{Lp} A_{mp} = U_{Ld} A_d \tag{22}$$

$$U_{Lr} A_r = U_{Ld} A_d \tag{23}$$

where U_{Lr}, U_{Ld} and U_{LP} are the superficial liquid velocities in the riser, downcomer and in the packing, respectively.

4.2.3. In the downcomer section

The energy dissipation due to stagnant gas in the downcomer (E_d) is obtained by performing an energy balance on the downcomer, using its liquid as the control volume, and also assuming that $\rho_L \gg \rho_g$:

$$E_d = \rho_L g h_D U_{Ld} A_d \varepsilon_{gd} \tag{24}$$

4.2.4. Frictional losses in riser and downcomer sections

The energy loss due to friction in the riser and downcomer (E_f) is given by the equation

$$E_f = \Delta P_{fr} U_{Lr} A_r + \Delta P_{fd} U_{Ld} A_d \tag{25}$$

where ΔP_{fr} and ΔP_{fd} are the frictional pressure drop due to fluid circulation flow through the riser and downcomer regions.

4.2.5. In the packed zone inside the downcomer section

By analogy with pipe flow and because of the continuity relationship between the downcomer (Eq. (22)) and gaps between adjacent fiber surfaces in the fibrous-bed (Eq. (25)), the energy dissipation rate in the packed bed (E_p) can be given by equation

$$E_p = \frac{1}{2} f_p \frac{\rho_l U_{Lr}^3 A_r}{(1-\varepsilon_{gd})^2}\left(\frac{A_r}{A_{Cp}}\right)^2 + U_{Lr} A_r \Delta P_p \tag{26}$$

where f_p is the loss coefficient due to fluid contraction from the top section of downcomer to the channels between the plates, A_{mp} is the cross-sectional area of flow through the packing, ΔP_p is the pressure drop through the bed. Substitution of Eqs. (20)–(26) into Eq. (18) gives:

$$\begin{aligned} 0 = {} & -\rho_L g h_D \varepsilon_{gr} + \rho_L g h_D \varepsilon_{gd} + \Delta P_{fr} + \Delta P_{fd} + \Delta P_{fP} \\ & + \frac{1}{2} f_P \rho_L U_{Lr}^2 \left(\frac{A_r}{1-\varepsilon_{gd}}\right)^2 \left(\frac{A_r}{A_{m_p}}\right)^2 \\ & + \frac{1}{2}\rho_L U_{Lr}^2 \left\{ f_b \left(\frac{2A_r}{A_d + (A_r - A_d)[1-(\varepsilon_{gr}+\varepsilon_{gd})]}\right)^2 \right. \\ & \left. + f_t \left(\frac{2A_r}{A_r + (A_r - A_d)[1-(\varepsilon_{gS}+\varepsilon_{gr})]}\right)^2 \right\} \end{aligned} \tag{27}$$

Eq. (27) is the basis of the method for the prediction of the liquid circulation rate, and requires a knowledge of the riser gas holdup (ε_{gr}) which depends on the superficial gas velocity (U_{gr}) and the liquid flow velocity (U_{Lr}), according to the equation cited Chisti et al. [20] and Chisti and Moo-Young [21] and given below in a rearranged form:

$$\varepsilon_{gr} = \frac{U_{gr}}{0.24 + 1.7 U_T^{0.7}} \tag{28}$$

Eq. (29) applies to air-water system when U_T ($=U_{Lr} + U_{gr}$) < 1.3 m s^{-1}.

The energy available for liquid motion described in Eq. (20) sets the liquid into circulation through the riser and the packed zone with a velocity u_{lLd} and hence this energy is totally dissipated at the liquid-packing interface. Thus, the net pressure drop (ΔP_P) for single-phase flow through a packed bed of more open or porous structures such as fibers, foam, or sponge elements having rough surfaces as described by De Nevers [43] is better described by a modified semi-empirical Ergun equation (porous packing elements having rough surfaces is given by

$$\Delta P_p = \frac{1}{2}\frac{f_p}{r_h}\rho_L u_{lLd}^2 L_p \tag{29}$$

or

$$\Delta P_p = \left[22.5\mu_L U_{Lr}(1-\phi_p)S_\upsilon + 0.5\xi\frac{\rho_L U_{Lr}^2}{(1-\varepsilon_{gd})}\left(\frac{A_r}{A_{mp}}\right)\right] \times \left(\frac{A_r}{A_{mp}}\right)\frac{L_P S_\upsilon (1-\phi_p)}{(1-\varepsilon_{gd})\phi_p^3} \tag{30}$$

were

$$\left.\begin{aligned} r_{h,d} &= \frac{\phi_p}{S_\upsilon(1-\phi_p)}, \\ u_{lLd} &= \frac{U_{Lp}}{(1-\varepsilon_{gd})\phi_p}, \\ f_p &= \frac{\Phi}{Re_p} + \xi, \\ Re_p &= \frac{4 r_h u_{lLd}\rho_L}{\mu_L} \end{aligned}\right\} \tag{31}$$

The Reynolds number (Re_p) of the packing element, Φ, and ξ are empirical constants which depends on the surface properties of the

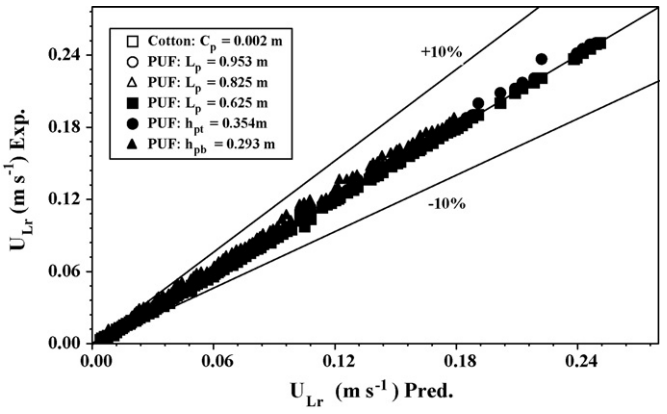

Fig. 13. Comparison of experimental and predicted riser liquid circulation velocity in the ILALB with packing.

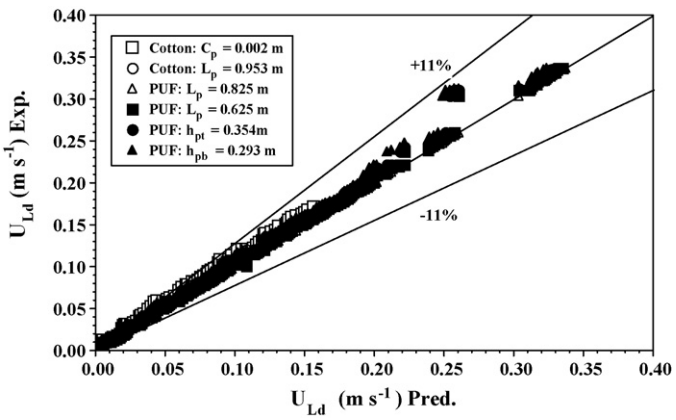

Fig. 14. Comparison of experimental and predicted downcomer liquid circulation in the ILALB with packing.

packing. The physical significance of Φ and ξ is to characterize the flow type in the packing. The values of the frictional pressure drops in the riser (ΔP_{fr}) and downcomer (ΔP_{fd}) sections for use in Eq. (27) may be calculated according to the procedure reported by Kilonzo et al. [11] and Kochbech and Hempel [42] for internal loop airlift bioreactors. Thus, substituting the values of ΔP_{fr}, ΔP_{fd}, and Eq. (30) into Eq. (27) leads to once again to an expression (32):

$$U_{Lr} = \left[\frac{2gh_D\left(\varepsilon_{gr} - \varepsilon_{gd}\right)}{f_r + f_T\left(\frac{2A_r}{A_r + (A_r - A_d)\left[1 - \left(\varepsilon_{gS} + \varepsilon_{gr}\right)\right]}\right)^2 + f_b\left(\frac{2A_r}{A_d + (A_r - A_d)\left[1 - \left(\varepsilon_{gr} + \varepsilon_{gd}\right)\right]}\right)^2 + f_d\left(\frac{A_r}{A_d}\right)^2 + f_P\left(\frac{A_r}{1-\varepsilon_{gd}}\right)^2\left(\frac{A_r}{A_d}\right)^2 + \left(1-\varepsilon_{gd}\right)\left(\frac{A_r}{A_d}\right)^2 \xi L_P S_\upsilon \frac{1-\phi_P}{\phi_P^3}} \right]^{0.5} \quad (32)$$

which may be solved for U_{Lr} to predict the liquid circulation velocity in ILALFBB The prediction of liquid circulation rate by using Eq. (32) would depend entirely on the surface properties of the packing elements and the value of ξ, where $\xi = 1.80$ for smooth surfaces, $\xi = 4.0$ for rough surface materials [43,44], and whether the flow is laminar ($Re_p < 10$). In Eq. (32), the values of the parameter f_b, f_t and f_p have been calculated by a procedure described by Kilonzo et al. [9].

Eq. (32) was used to predict the liquid circulation velocity at different operating conditions. Figs. 13 and 14 shows the comparison between experimental and predicted values of the riser and downcomer liquid circulation velocities, respectively in the bioreactor. It has clearly shown in Figs. 13 and 14 that the present model can predict the liquid circulation velocity in the fibrous packed bed ILALB with satisfactory accuracy (the deviation is ±10% and ±11% for the riser and downcomer, respectively).

4.3. Correlation of mass transfer coefficient K_La

The mass transfer coefficient (K_La) was correlated with superficial gas velocity in the riser (U_{gr}) because the gas flow provided not only the dispersed gas phase but also the power input into the airlift bioreactor. For the packed downcomer, the following correlation equations are presented for the mass transfer coefficient.

Correlation ($R = 0.938$, $R^2 = 0.843$, S.E. = 0.0002) for packed downcomer:

$$K_La = 34700\left(\frac{D_L}{d_d^2}\right)\left(\frac{U_{gr}}{d_S}\right)^{0.09}\left(\frac{h_{Pb}}{d_d}\right)^{0.78}\left(\frac{h_{Pt}}{d_d}\right)^{-0.39}\left(\frac{L_P}{d_d}\right)^{0.69} \times \left(\frac{\rho_L^2 g d_d^3}{\mu_L^2}\right)^{0.33}\left(\frac{m_P}{d_d}\right)^{-0.34}\left(\frac{d_s}{d_d}\right)^{-5.7} \quad (33)$$

Correlations (33) was based on data within the ranges given in Eq. (17). Correlation Eq. (33) was found to apply to the proposed bioreactor configuration as shown in Fig. 15 for the air–water system used.

The correlation can predict the mass transfer coefficient in the proposed bioreactor system (ILALB with fibrous-bed) with a deviation of ±37% for the K_La. Clearly, from Figs. 8–10, the fiber and polymer packing did improve K_La at any given gas flow (and hence fixed power input) relative to the ILALB configuration without the packing. The correlation was based on 147 data, each representing the average of a duplicated experiment. The correlation shows an exponent of 0.09 on the term $[U_{gr}/d_s]$. The influence of the gap between fiber surfaces m_p, represented by $[m_p/d_d]$, reflects the increase in mass transfer rate expected from an increase in gas holdup and interfacial area. The negative exponent applied to the rage of variation of $[m_p/d_d]$, would give an increase of K_La by a 21% for the maximal gap width range tested. The influence of apparent viscosity, represented by the term $[g\rho_L^2 d_d^2/\mu_L]$, had no significance on K_La since it was a fixed variable. Both the top h_{Pt} and bottom h_{Pb} clearances of the bed affect the mass transfer rate in modest proportions. Considering the range of variations of $[h_{pb}/d_d]$ is one order of magnitude, the correlation provides a maximal decrease of $10^{-0.088}$ approximately 18%. The same analysis gives a maximal change of around 36% due to the bed top clearance variation in $[h_{pt}/d_d]$. The

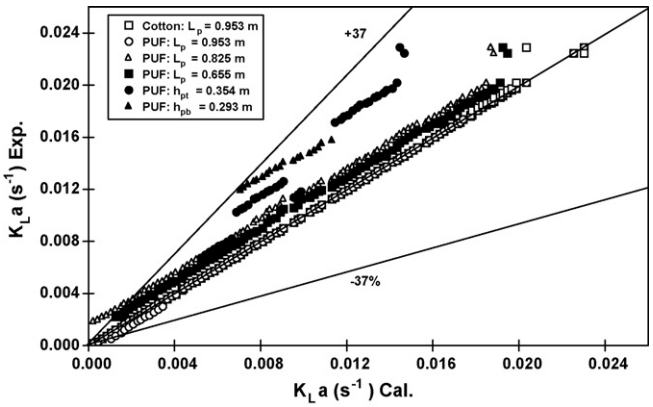

Fig. 15. Parity plot of experimentally obtained values of the $K_L a$ vs. those calculated from correlation (34) for the ILALB with packing, and within the data range given in Eq. (18) (h_L = 1.208 m, L_d = 1.024 m, h_t = 0.156 m, h_b = 0.060 m).

influence ascribed to the bubble disengagement group, $[d_S/d_d]$, has a maximal influence of up to 65%.

The influence of the gap width, m_p, represented by the term $[m_p/d_d]$, reflects the increase in mass transfer rate expected due to the continuous breakup of the gas bubbles into smaller sizes with increased interfacial area. The negative exponent applied to the experimental values tested; gave an increase of $K_L a$ by about 80%. The influence of packing height represented by the slenderness ratio $[L_p/d_d]$, has significant effect too, to the mass transfer coefficient.

The correlations obtained in this work indicate that gas holdup behaves linearly, as compared to the liquid circulation velocity and mass transfer coefficient. This may be understood due to the increased downcomer gas holdup in the experiment considered in this work.

5. Conclusion

Hydrodynamic and the mass transfer performance in an ILALB with cotton and or polyurethane foam (PUF) packing in the downcomer (draft tube) section have been measured and modeled. The dependence of gas holdup, liquid circulation velocity, and mass transfer coefficient on the packing nature, packing height, gap width between fiber surfaces, bed's top and bottom clearances, and superficial gas velocity was significant. Gas holdup and $K_L a$ values continuously increased with decrease in gap width, but with increases in both packing height and bed's top clearance. This was associated with the increase in the interfacial area due to the shearing action of the fibrous-bed. Increased amounts of packing in the ILALB, whether cotton or polyurethane foam in the form of height with large top clearance and narrow gap width, decreased the liquid circulation velocity in the ILALB because of increased frictional resistance, tortuosity, and baffling action of the bed. Empirical correlations are presented which accurately predict gas holdup, liquid circulation velocities, and volumetric mass transfer coefficient as a function of all five independent variables (packing nature, packing height, bed's top and bottom clearances, gap width, and gas velocity). It is concluded that, under the hydrodynamic conditions for a fibrous-bed packed ILALB occur at full cotton packing (porosity: 0.96) and minimum PUF packing (porosity: 0.96) with large top clearance and 0.004 m gaps between fiber surfaces. These conditions will allow not only, highest gas holdup to improve mass transfer, but also high cell loading and large void space to reduce clogging and liquid frictional losses.

Acknowledgements

The support by the Natural Science and Engineering Research Council of Canada (NSERC) is acknowledged through individual research grants awarded to Dr. A. Margaritis and Professor M.A. Bergougnou.

References

[1] C. Wei, B. Xie, H. Xiao, D. Wang, Volumetric mass transfer coefficient of oxygen in an internal loop airlift reactor with a convergence-divergence draft tube, Chem. Eng. Technol. 23 (2002) 5974–6603.
[2] M.R. Mehrnia, B. Bonakdarpour, J. Towfighi, M.M. Akbarnejad, Design and operational aspects of airlift bioreactors for petroleum biodesulfurization, Envion. Prog. 23 (3) (2004) 206–214.
[3] Y. Chisti, U.J. Jauregui-Haza, Oxygen transfer and mixing in mechanically agitated airlift bioreactors, Biochem. Eng. J. 10 (2002) 143–153.
[4] J.P. Wen, X. Jia, X. Cheng, P. Yang, Characteristics of three-phase internal loop airlift bioreactors with complete gas recirculation for non-Newtonian fluids, Bioproc. Biosyst. Eng. 27 (2005) 193–205.
[5] J.P. Wen, X.Q. Jia, W. Feng, Hydrodynamic and mass transfer of gas-liquid-solid three-phase internal loop airlift reactors with nanometer particles, Chem. Eng. Technol. 28 (1) (2005) 53–60.
[6] W.A.J. Benthum, R.G.J.M. van der Lans, M.C.M. van Loosdretcht, J.J. Heijnen, The biolfilm airlift suspension extension reactor–II: Three-phase hydrodynamics, Chem. Eng. Sci. 55 (2000) 699–711.
[7] J. Klein, A.A. Vicente, J.A. Teixeira, Hydrodynamic considerations on optimal design of a three-phase airlift bioreactor with high solids loading, J. Chem. Technol. Biotechnol. 78 (2003) 935–944.
[8] M. Deront, M. Falilou, S.N. Adler, P. Peringer, Volumetric oxygen mass transfer coefficient in upflow concurrent packed-bed bioreator, Chem. Eng. Sci. 53 (1998) 1321–1330.
[9] P. Kilonzo, A. Margaritis, M.A. Bergougnou, Airlift-driven fibrous bed bioreactor for continuous production of glucoamylase using immobilized recombinant yeast cells, J. Biotechnol. 1217 (1) (2006) 17–26.
[10] M. Gavrilescu, R.Z. Tudose, Modellong of liquid circulation in concentric-tube airlift reactors, Chem. Eng. J. 69 (1998) 85–91.
[11] P. Kilonzo, A. Margaritis, M.A. Bergougnou, J.T. Yu, Q. Ye, Effects of Geometrical Design on Hydrodynamics and Mass Transfer Characteristics of a Rectangular Column Airlift Bioreactor, Biochem. Eng. J. 34 (3) (2007) 279–288.
[12] L. Jiang, J. Wang, S. Liang, X. Wang, P. Cen, P. Xu, Butyric acid fermentation in a fibrous-bed bioreactor with immobilized *Clostridium tyrobutyricum* from cane molasses, Bioresource Technol. 100 (2009) 3403–3409.
[13] Z.-N. Xu, S.-T. Yang, Production of mycophenolic acid by *Penicillium brevicompactum* immobilized in a rotating fibrous-bed bioreactor, Enzyme Microbial. Technol. 40 (2007) 623–628.
[14] P. Kilonzo, A. Margaritis, M.A. Bergougnou, Airlift-driven fibrous-bed bioreactor for continuous production of glucoamylase using immobilized recombinant yeast cell, J. Biotechnol. 143 (3) (2009) 60–68.
[15] P.M. Kilonzo, Ph.D. Thesis, University of Western Ontario, London, Ontario, Canada. A novel fibrous bed airlift bioreactor for recombinant yeast fermentation, 2009.
[16] C.H. Hsu, Y.E. Chu, S. Argin-Soyal, T.S. Hahm, Y.M. Lo, Effects of surface characteristics and xanthan polymers on the immobilization of *xanthomonas Campestris* to fibrous matrices, J. Food Sci. 69 (9) (2004) E441–E448.
[17] T. Ma, S.-T. Yang, D.A. Kniss, Development of an invitro human placenta model by cultivation of human trophoblasts in a fiber-based bioreactor system, Tiss. Eng. 5 (1999) 91–102.
[18] Y. Huang, S.-T. Yang, Acetate production from whey lactose using co-immobilized cells of homolactic and homoacetic bacteria in a fibrous-bed bioreactor, Biotechnol. Bioeng. 60 (1998) 499–507.
[19] J.S. Melo, S.F. D'Souza, Simultaneous filtration and immobilization of cells from a flowing suspension using a bioreactor containing polyethylenimine coated cotton threads: application in the continuous inversion of concentrated sucrose syrups, World J. Microbiol. Biotechnol. 15 (1) (1999) 23–27.
[20] Y. Chisti, M. Kasper, M. Moo-Young, Mass transfer in external loop airlift bioreactors using static mixers, Can. J. Chem. Eng. 68 (1990) 38–45.
[21] Y. Chisti, M. Moo-Young, Airlift bioreactors with packed beds of immobilized biocatalysts: Theoretical evaluation of the liquid circulation performance, Trans. Inst. Chem. Engrs. 71 (Part C) (1993) 209–212.
[22] K. Okada, Y. Nagata, Y. Akagi, Effect of packed bed on mass transfer in external loop-airlift bubble column, J. Chem. Eng. Jpn. 29 (4) (1996) 582–587.
[23] H. Nikakhtari, G.A. Hill, Hydrodynamic and oxygen mass transfer in an external loop airlift bioreactor with a packed bed, Biochem. Eng. J. 27 (2005) 138–145.
[24] H. Nikakhtari, G.A. Hill, Enhanced oxygen mass transfer in an external loop airlift bioreactor using a packed bed, Ind. Eng. Chem. Res. 44 (2005) 1067–1072.
[25] M. Martinov, D. Hadjiev, S.D. Vlaev, Gas-liquid mass transfer in fibrous bed reactor with counter-current liquid recycle, Chem. Eng. Technol. 32 (6) (2009) 1–8.

[26] T.-W. Chiou, S. Murakami, I.C. Wang, A fiber-bioreactor for anchorage-dependent animal cell culture: Part I. Bioreactor design and operation, Biotechnol. Bioeng. 37 (1991) 755–761.
[27] P.D. Gaspillo, S. Goto, Mass transfer in slurry bubble column with static mixer in draft-tube, J. Chem. Eng. Jpn. 24 (1991) 680–682.
[28] G.-L. Guo, D.-H. Tseng, S.-L. Huang, Co-metabolic degradation of trichloroethylene by *Pseudomonas putida* in a fibrous bed bioreactor, Biotechnol. Lett. 23 (2001) 1653–1657.
[29] P.-M. Wang, T.-K. Huang, H.-P. Cheng, Y.-H. Chien, W.T. Wu, A modified airlift reactor with high capabilities of liquid mixing and mass transfer, J. Chem. Eng. Jpn. 35 (2002) 354–359.
[30] J. Korpijarvi, P. Oinas, J. Reunanen, Hydrodynamics and mass transfer in an airlift reactor, Chem. Eng. Sci. 54 (1999) 2255–2262.
[31] E.E. Petersen, A. Margaritis, Hydrodynamic and mass transfer characteristics of three-phase gaslift bioreactor system, Crit. Rev. Biotechnol. 21 (4) (2001) 233–294.
[32] B. Bhatia, K.D.P. Nigam, D. Auban, G. Herbrard, Effect of a new high porosity packing on hydrodynamics and mass transfer in bubble columns, Chem. Eng. Proc. 43 (2004) 1371–1380.
[33] S. Moustiri, G. Herbrard, M. Rousten, Effect of a new high porosity packing on hydrodynamics of bubble columns, Chem. Eng. Proc. 41 (2001) 419–426.
[34] M.E. Abashar, U. Narsingh, A.E. Rouillard, R. Judd, Hydrodynamic flow regimes, gas holdup, and liquid circulation in airlift reactors, Ind. Eng. Chem. Res. 37 (1998) 1251–1263.
[35] X. Jia, J. Wen, Y. Jiang, X. Liu, L.W. Feng, Modeling of batch phenol biodegradation in internal loop airlift bioreactor with gas recirculation by *Candida tropicallis*, Chem. Eng. Sci. 61 (2006) 3463–3475.
[36] A.X. Meng, G.A. Hill, A.K. Dalai, Hydrodynamic characteristics in an external loop airlift bioreactor containing a spinning sparger and a packed bed, Ind. Eng. Chem. Res. 41 (2004) 2124–2128.
[37] X. Su, T.J. Heindel, Gas holdup in nylon fiber suspensions, Ind. Eng. Chem. Res. 43 (2004) (2004) 2256–2263.
[38] J.H.J. Kluytmans, B.G. van Wachem, B.M. Kuster, J.C. Schouten, Gas holdup in a slurry bubble column: Influence of electrolyte and carbon particles, Ind. Eng. Chem. Res. 40 (2001) 5326–5338.
[39] V. Höller, D. Wegricht, L. Kiwi-Minsker, A. Renken, Fibrous structured catalytic beds for three-phase reaction engineering hydrodynamics study in staged bubble columns, Catal. Today 40 (2000) 51–56.
[40] V. Höller, K. Radevik, L. Kiwi-Minsker, A. Renken, Bubble columns staged with structured fibrous catalytic layers: Residence time distribution and mass transfer, Ind. Eng. Chem. Res. 40 (2001) 1575–1579.
[41] S. Kim, M.A. Deshusses, Determination of mass transfer coefficients for packing materials used in biofilters and biotrickling filters for air pollution control, Chem. Eng. Sci. 63 (2008) 841–855.
[42] B. Kochbech, D.C. Hempel, Liquid velocity and dispersion coefficient in an airlift reactor with inverse internal loop, Chem. Eng. Technol. 17 (1994) 401–405.
[43] N. de Nevers, Flow through Porous Media: In Fluid Mechanics for Chemical Engineers, second ed., McGraw-Hill, Inc., New York, 1991, pp. 410–432.
[44] J.M.A. Young, R.G. Carbonell, D.F. Ollis, Airlift Bioreactors: analysis of local two-phase hydrodynamics, AIChEng. J. 37 (3) (1991) 403–428.